Journal of Alloys and Compounds 509 (2011) 3735–3739

Contents lists available at ScienceDirect

Journal of Alloys and Compounds

journal homepage: www.elsevier.com/locate/jallcom

Electronic and thermal properties of non-magnetic CeRhGa

Jerzy Goraus*, Andrzej Ślebarski, Marcin Fijałkowski

Institute of Physics, University of Silesia, 40-007 Katowice, Poland

ARTICLE INFO

Article history:
Received 17 November 2010
Received in revised form
22 December 2010
Accepted 25 December 2010
Available online 31 December 2010

Keywords:
Rare earth alloys and compounds
Thermodynamic properties
Electronic band structure
Crystal structure

ABSTRACT

The magnetic and electric transport properties of the orthorhombic CeRhGa compound have been determined from the analysis of magnetic susceptibility, magnetization vs magnetic field, specific heat and electrical resistivity. The atomic positions and the lattice parameters were refined from Rietveld analysis. From our thermodynamical studies, CeRhGa is paramagnetic compound with valence instability of the 4*f* shell of Ce. X-ray photoelectron spectroscopy (XPS) measurements also confirm a mixed valent character of Ce and strong onsite hybridization between 4f and conduction electron states in the band. Band structure calculations give nonmagnetic ground state for CeRhGa and a good agreement between the measured valence band XPS spectra and the calculated bands.

1. Introduction

Ternary intermetallic cerium compounds, CeTX, where T and X represent transition metal and p-electron atoms, respectively are amongst often studied systems due to their relatively simple crystallographic structure and a variety of different ground states, which are manifested in a range of electronic and magnetic properties which they exhibit. Various ground states sensitively depend on the balance between the on-site Kondo and the intersite Ruderman–Kittel–Kasuya–Yosida (RKKY) exchange interactions. Generally, the coupling constant J_{fs}, between the localized 4f spins and the conduction electron spins as well as the hybridization energy between the 4f and the conduction electron states V_{fs}, determine their ground state properties.

Studies of CeTX, where T is a transition metal and X is Sb, Sn, Ga, or Al also provide an opportunity to investigate the effect of variation of J_{fs} by varying T or X element on the magnetic/nonmagnetic properties of the ground state. For the series of elements: Sb, Sn, Ga, and Al an atomic radius systematically increases, therefore the CeTAl or CeTGa compounds are expected to be magnetic, which indeed has been reported [1], excluding CeRhGa. CeRhGa crystallizes in an orthorombic TiNiSi-type structure [2] and was reported as a non-magnetic compound with an intermediate valent behaviour. Most recently, the intermediate valence character of CeRhGa was corroborated by the x-ray diffraction analysis, which motivated us to undertake our detailed investigations of this compound. In this article, we report the crystallographic data from x-ray diffraction analysis and the results of magnetic, electric transport, specific heat, and XPS studies on CeRhGa. The compound was found to exhibit behaviour typical of strongly correlated electron systems, such as enhanced linear contribution to a specific heat, an intermediate valence of Ce, and the field dependence of the magnetoresistivity. We also found that CeRhGa exhibits characteristic Landau Fermi-liquid-like metallic properties with only exception being the resistivity, which is well explained by the parallel resistor model [3].

2. Experimental and calculation details

Polycrystalline CeRhGa sample was prepared by arc melting the constituent elements on a water cooled copper hearth in a high-purity argon atmosphere with an Al getter. The sample was remelted several times to promote homogeneity and annealed at 800 ° C for 2 weeks. The powder diffraction pattern was measured on Rigaku-Denki D/MAX RAPID II-R diffractometer (Rigaku Corporation, Tokyo, Japan) with a rotating anode Ag K_α tube ($\lambda = 0.5608$ Å), an incident beam (0 0 2) graphite monochromator and an image plate in the Debye-Scherrer geometry. XRD data were refined using FULLPROF program [4] with pseudo-Voigt line shape, the refined atomic positions and lattice parameters are given in Table 1. These parameters were also used in our band structure calculations. The X-ray powder-diffraction pattern of the samples did not show the presence of any impurity phases.

Thermodynamic properties were measured with Quantum Design Physical Properties Measurement System (QD-PPMS): resis-

* Corresponding author.
E-mail addresses: jerzy.goraus@us.edu.pl (J. Goraus), andrzej.slebarski@us.edu.pl (A. Ślebarski), marcin.fijalkowski@us.edu.pl (M. Fijałkowski).

0925-8388/$ – see front matter © 2010 Elsevier B.V. All rights reserved.
doi:10.1016/j.jallcom.2010.12.183

Table 1
Rietveld refinement results for CeRhGa (space group *Pnma*); lattice parameters: $a = 6.8512(26)$ Å, $b = 4.3726(16)$ Å, $c = 7.8458(26)$ Å, the atomic positions are listed in the table.

atom	x	y	z
Ce	0.5321(24)	0.25	0.3124(20)
Rh	0.1517(36)	0.25	0.5699(27)
Ga	0.7553(56)	0.25	0.6183(43)

tivity with AC transport (ACT), susceptibility and magnetization with VSM (vibrating sample magnetometer) and heat capacity with He^3 option. Resistivity and specific heat were measured down to 0.5 K. Magnetic susceptibility $\chi(T)$ was measured at $B = 0.1$ T down to 1.9 K.

FP-LAPW (full potential, linear augmented plane wave) band structure calculations were performed using version 1.1.04 of Elk FP-LAPW [5] code with 120 *k*-points in irreducible Brillouin Zone. We have chosen PBEsol GGA (generalized gradient approximation) [6] exchange-correlation potential (V_{xc}) as it is considered to depict more properly elastic properties and equilibrium lattice parameters of solids than standard LSDA (local spin density approximation). We used muffin-tin radius $R_{MT} = 2.45$ a.u. (atomic unit) for Ce, 2.35 a.u. for Rh and 2.22 a.u. for Ga. Calculations were carried out in a collinear magnetic mode, with magnetization direction across *z*-axis.

For a comparison of experimental valence band X-ray photoemission spectroscopy (VB-XPS) spectrum with our theoretical results we used the following procedure: calculated partial densities of states (DOS) were summed across corresponding Wyckoff sites and multiplied by a proper crossection take form [7], these weighted total DOS was then convoluted with Lorentztian line shape (FWHM = 0.4 eV) for consideration of finite life time and experimental resolution.

3. Results and analysis

3.1. Magnetic susceptibility

Fig. 1 shows the magnetic susceptibility χ (VSM) measured as a function of temperature in the magnetic field of 0.1 T. Above $T = 50$ K the magnitude of susceptibility is small ($\sim 10^{-3}$ emu/mol)

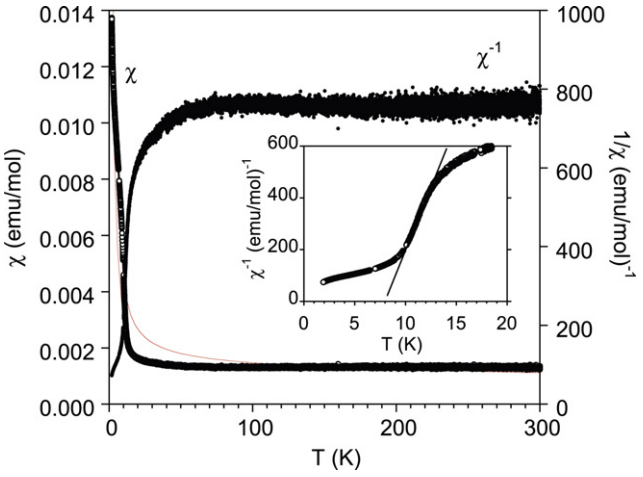

Fig. 1. Magnetic susceptibility (VSM) χ and χ^{-1} in the magnetic field of 0.1 T vs. temperature *T*. The dotted line in the figure represents the $\chi(T) = \chi_0 + \gamma C/T + nC/(T-\theta) + N_A\mu^2 n_f/3k_B(T+T_{sf})$ fit based on the ICF model with $\chi_0 \approx 3 \times 10^{-4}$ emu/mol, a fraction of paramagnetic Ce impurities $y \sim 0.02$, $n \sim 1 \times 10^{-3}$, and large interconfigural fluctuation temperature $T_{sf} \sim 500$ K between the configurations f^1 and f^0 of Ce. The inset shows the Curie–Weiss fit to the impurity contribution in $1/\chi$ vs *T* data.

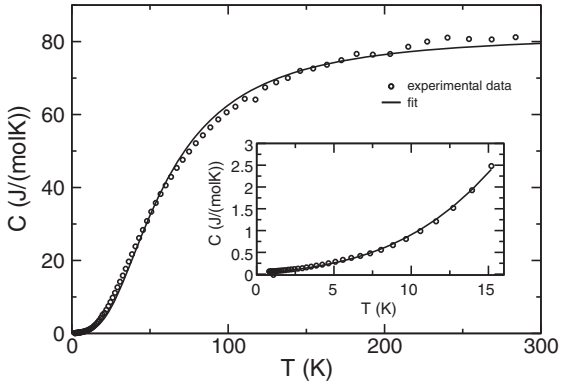

Fig. 2. Specific heat (circles) compared with the fit to full Debye expression (solid line). The inset shows the low-temperature specific heat data between 0.5 K and 15 K and a fit of $C(T) = \gamma T + \beta T^3$ (line) with the parameters $\gamma \sim 38.3$ mJ/(mol K^2), $\beta \sim 5.2 \times 10^{-4}$ mJ/(mol K^4).

and $\chi(T)$ is not temperature dependent, while below 15 K it has a Curie–Weiss behaviour ($\chi = nC/(T-\theta)$) due to a very small amount of the magnetic impurity phase with $n \sim 0.01$ and Curie–Weiss temperature $\theta \approx 8$ K (cf. the inset to Fig. 1). The effective magnetic moment $\mu_{eff}(T) = (3k_B/N_A)^{1/2}(\chi T)^{1/2}$ per one Ce atom is about 1.5 μ_B at $T = 300$ K (not shown in Fig. 1), which is less than the Hund's rule value 2.54 μ_B of the free ion Ce^{3+}. The ionic two-level interconfiguration fluctuation (ICF) model proposed by Sales and Wohlleben [8] can determine how much of the susceptibility reported in Fig. 1 is intrinsic. The solid line in the figure represents the $\chi(T) = \chi_0 + \gamma C/T + nC/(T-\theta) + N_A\mu^2 n_f/3k_B(T+T_{sf})$ fit based on the ICF model with $\chi_0 \approx 3 \times 10^{-4}$ emu/mol, a fraction y of paramagnetic Ce impurities ~0.02, $n \sim 1 \times 10^{-3}$, and large interconfigural fluctuation temperature ($T_{sf} \sim 500$ K) between the configurations f^1 and f^0. The magnetization *M* measured at $T = 2$ K is linear with magnetic field *H* at the fields $3 < |H| < 9$ T, while in smaller fields *M* shows a weak impurity effect in $M(H)$ dependence with remanence of about 8×10^{-3} μ_B at $H = 0$. Magnetic susceptibility $\chi(T)$ and the low-*T* magnetization $M(H)$ behaviours in CeRhGa are typical for a cerium valence-fluctuation compound.

3.2. Specific heat and electrical resistivity

Fig. 2 displays the specific heat in zero magnetic field versus temperature in wide temperature range. The low-temperature specific heat is well approximated by expression $C(T) = \gamma T + \beta T^3$, with $\gamma \sim 38.3$ mJ/(mol K^2) and $\beta \sim 5.2 \times 10^{-4}$ mJ/molK^4, which corresponds to Debye temperature $\Theta_D \sim 223$ K when three atoms (n) in formula unit are assumed. The relatively small value of γ obtained for CeRhGa is characteristic of non-magnetic mixed valent Ce-compounds [9]. It seems for us surprising that $C(T)$ can be well fitted by full Debye expression

$$C_p = 9Rn_D(T/\Theta_D)^3 \int_0^{\Theta_D/T} \frac{x^4 e^x}{(e^x - 1)^2}\, dx$$

in the wide temperature range, when the crystal-field contribution is neglected. The least-square fit of the lattice contribution to the experimental data $C(T)$ yield a reasonable value of Debye temperature $\theta_D \sim 239$ K and number of atoms in formula unit $n_D \sim 3.28$. A good quality of the fit and the value of n_D which is essentially equal to assumed composition lead us to conclusion that the contribution of crystal field effect to specific heat of CeRhGa is small.

Fig. 3 displays the low-temperature specific heat C/T of CeRhGa in several magnetic fields. In an applied magnetic field, C/T is suppressed and levels off towards a constant value as $T \to 0$. We note, that for $0.8 < T < 3$ K C/T shows divergent character and power-law

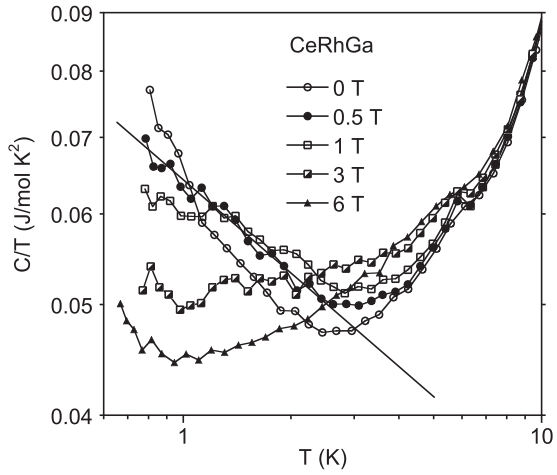

Fig. 3. Specific heat C divided by T, $C(T)/T$ at different magnetic fields H in a log–log scale. In an external field $H = 0.5$ T $C(T)/T \sim T^{-n}$, $n = 0.27$ below ~3 K.

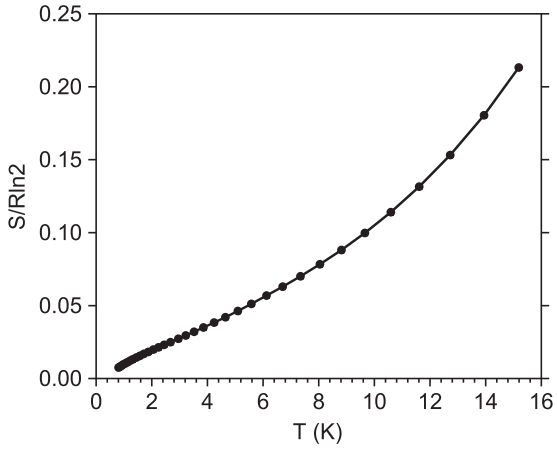

Fig. 4. Low-temperature entropy $S/Rln2$ for CeRhGa. In the low-T range (for $T < 8$ K) $S \sim T$.

behaviour at $B = 0.5$ T. In the low-temperature metallic state the entropy $S \sim \gamma T$ and is much less than the value of $Rln2$ expected for a doublet ground state (see, Fig. 4).

As seen in Fig. 5, the electrical resistivity $\rho(T)$ shows metallic conductivity, well approximated by parallel resistor model (PRM)

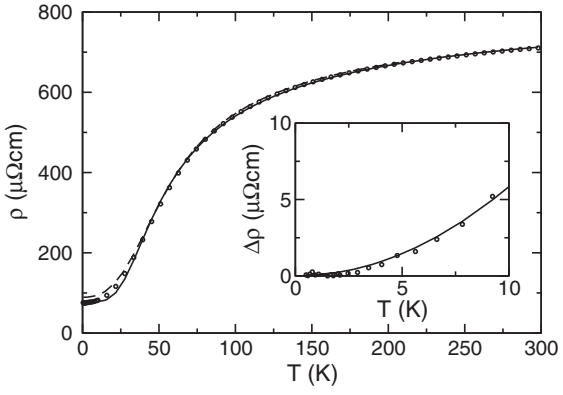

Fig. 5. Electrical resistivity ρ measured in external magnetic fields $H = 0$ (open points) and $H = 9$ T (dashed line), and a fit of the PRM function to the experimental data obtained in the field $H = 0$. The inset displays the low-temperature $\rho(T)$-data subtracted by the residual resistivity ρ_0 ($\Delta\rho(T) = \rho(T) - \rho_0$). The $\Delta\rho$ data are well fitted by the function $\Delta\rho(T) = AT^2$ with $A \sim 0.0584\ \mu\Omega$cm/T^2.

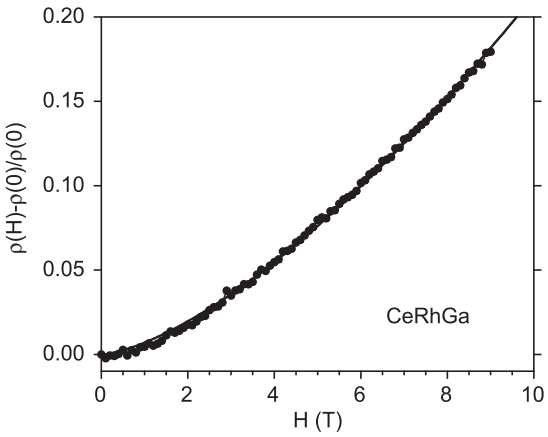

Fig. 6. Magnetoresistivity $[\rho(H) - \rho(0)]/\rho(0)$ vs. magnetic field at $T = 2$ K. The continous line shows a fit of $[\rho(H) - \rho(0)]/\rho(0) \sim H^{1.41}$ to the experimental data.

[3] with the fitting formula:

$$\rho(T) = \rho_0 + \frac{\rho_{ph} \cdot \rho_{\max}}{\rho_{ph} + \rho_{\max}},$$

where

$$\rho_{ph} = 4RT\left(\frac{T}{\Theta_D}\right)^4 \int_0^{\frac{\Theta_D}{T}} \frac{x^5 dx}{(e^x - 1)(1 - e^{-x})}$$

is the phonon part of ρ (Bloch-Grüneisen function), ρ_0 is the residual resistivity and $\rho_{\max}$ is the saturation resistivity which is independent of temperature. We obtained the following fit parameters: $\rho_0 = 78.16\ \mu\Omega$cm, $\rho_{\max} = 741.75\ \mu\Omega$cm, $R = 348\ \mu\Omega$cm/ K and $\Theta_D = 193.2$ K. In the inset to Fig. 5 the low-temperature electrical resistivity $\rho(T)$ is well described by a formula $\rho = \rho_0 + AT^2$, with $\rho_0 \sim 75.5\ \mu\Omega$cm and $A \sim 0.0584\ \mu\Omega$cm/K^2, characteristic of Fermi liquids. The obtained values of A and γ allowed us to locate CeRhGa on Kadowaki-Wood $A \sim \gamma(0)$ relation as a Fermi liquid state with enhanced density of states at the Fermi level. The non-magnetic and metallic character of CeRhGa is also shown in Fig. 6, which displays the positive magnetoresistivity $[\rho(H) - \rho(0)]/\rho(0) \sim H^{3/2}$ obtained at $T = 2$ K. The magnetoresistivity $\Delta\rho/\rho(0)$ is about 18% in the magnetic field of $B = 9$ T and at $T = 0.5$ K.

3.3. XPS spectra and the band structure calculations

The 3d-core-level XPS spectrum measured for CeRhGa is shown in Fig 7. The main components $3d^9_{5/2}4f^1$ and $3d^9_{3/2}4f^1$ originate

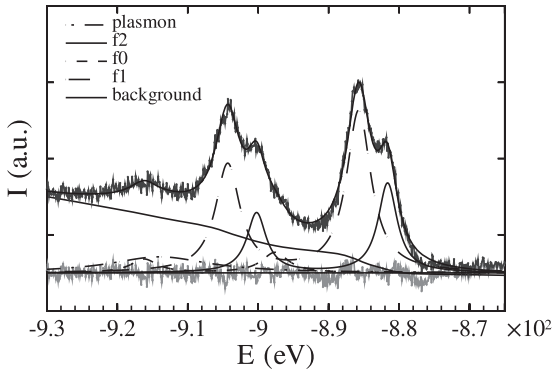

Fig. 7. Ce 3d XPS spectrum for CeRhGa and the components: $3d^94f^0$, $3d^94f^1$, and $3d^94f^2$ separated using Lorentzian line shape of each line and Shirley background. Deconvolution of the lines upon Gunnarson-Schönhammer theory gives the occupation number of the 4f shell $n_f \sim 0.9$ and the hybridization energy $\Delta \sim 150$ meV.

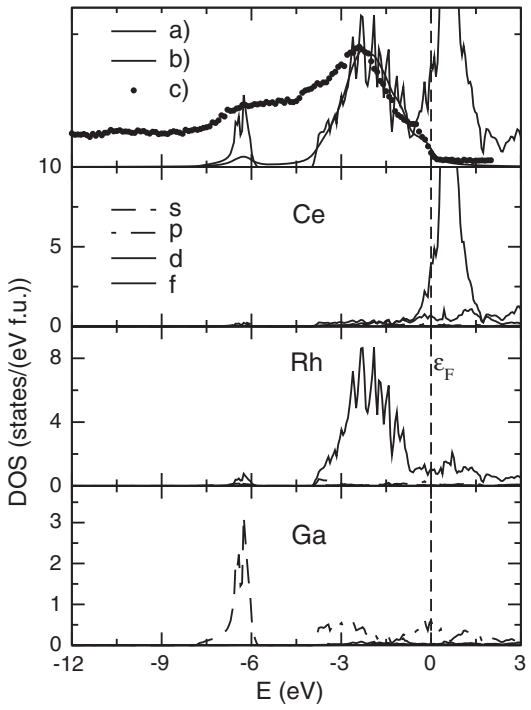

Fig. 8. Comparison of the total DOS calculated for paramagnetic CeRhGa (a) with the measured XPS valence bands [the XPS spectra, (c), are not corrected by the background]. Thick line (b) represents the convoluted sum of the partial DOSs multiplied by a proper cross-section coefficient. Theoretical XPS spectra (b) compared with experimental one (c) show good agreement. The lower panels of the figure show the contributions of Ce, Rh, and Ga atoms (with respect to the orbitals l = s,p,d,f) to the total DOS.

from Ce^{3+} ions and exhibit a spin–orbit splitting $\Delta_{SO} = 18.6$ eV, whereas appearance of the $3d^9 4f^2$ and $3d^9 4f^0$ components in the spectrum is a clear manifestation of intraatomic hybridization between the 4f states and the conduction band. The weak structure $3d^9 4f^0$ located about 11 eV away from the main peaks is due to the $3d^9 f^0$ component and hint at somewhat unstable character of the 4f shell. In turn, the $3d^9 4f^2$ final-state components are located on the low-energy side of the main lines at the distance of about 4 eV. They appear when the core 3d hole is screened by an additional 4f electron. From their contribution to the measured Ce 3d spectrum one can find the hybridization energy $\Delta = \pi V^2 N(E_F)$, which describes the hybridization part of the Anderson impurity Hamiltonian [10] (in the expression V is the hybridization matrix element and $N(E_F)$ is the density of states at the Fermi level). We used Lorentzian line shape and Shirley background [11] to determine the intensities of the contributed lines f^0, f^1, and f^2. Spin-orbit split of 18.6 eV was assumed for $j = 5/2$ and $j = 3/2$ Ce 3d XPS lines, their intensities 3:2 were also fixed with respect to their degeneracy ratio. The intensity ratio of the $3d4f^n$ components was performed based on the Gunnarson-Schönhammer (GS) theory (for detailes on the method applied see Ref. [12]). The ratio $I(f^2)/[I(f^1) + I(f^2)]$ yields a hybridization energy Δ of about 150 meV, while from the ratio $I(f^0)/[I(f^0) + I(f^1) + I(f^2)]$ the occupation of the 4f shell is roughly estimated to be $n_f \approx 0.9$. The obtained Δ and n_f are characteristic for Ce-compounds with valence instability (valence fluctuation) of the Ce ions and support the magnetic data for CeRhGa. Within the approximations inherent to the GS theory, some errors of ~20% in the determination of the hybridization strength and fractional valency of Ce is due to uncertainty in the proper intensity ratios $3d^9 4f^1 : 3d^9 4f^2 : 3d^9 4f^0$, directly related to the accuracy of decomposition of the spectrum, as well as to proper background subtraction.

Our band structure calculations gave an almost non-magnetic ground state of CeRhGa with magnetic moment on atoms and in the interstitial region lower than 0.02 μ_B. This result is in agreement with the experimental data.

In Fig 8 (upper plot) we compare the experimental and calculated VB-XPS spectra. The lower panel of the figure shows the partial DOSs for Ce, Rh and Ga electronic states. It is clear that the Rh-4d states and Ga-4s states mainly form the shape of the VB-XPS spectra, but the Ce-4f states are located in the vicinity of the Fermi energy in the total DOS.

The calculated value of DOS at E_F well corresponds to the value of the density of states experimentally obtained from the Sommerfeld coefficient γ [$\gamma_{calc} \sim 45$ mJ/(molK^2) is quite near to the experimental value of $\gamma_{exp} \sim 38$ mJ/(molK^2)]. This, rather untypical for a Ce-based compound agreement leads to the conclusion that the correlations between Ce-4f states are rather weak in CeRhGa.

Finally, we discuss the zero-field $C(T)/T$ results. In the single-ion theory the Kondo temperature T_K is related to the maximum value of γ at $T = 0$ by $\gamma_{\max} T_K \cong 0.68R$, where R is the gas constant. The T_K value obtained from $\gamma_{\max}$ at $T = 0.6$ K in this way [13] is $T_K \sim 70$ K. In the concentrated Kondo-lattice system this temperature rather signals a transition to the coherent state. The results for $\gamma(T)$ as a function of magnetic field presented in Fig. 3 provide further evidence for the Fermi-liquid behaviour. The $\gamma(T)$ is strongly reduced with an increasing of the field. Moreover, in the field of 0.5 T the scaling $C/T \sim T^{-n}$ is found in the one decade of T, it might signal possible non-Fermi liquid behaviour in this field, however, to qualify this behaviour, one needs to measure the specific heat in the lowest temperatures, i.e., well below 0.6 K.

3.4. Conclusions

CeRhGa is a mixed valent Ce compound with essentially quenched magnetic moment due to large hybridization between the 4f electrons with the conduction band. The relatively large hybridization effect leads to the valence instability of the f shell of Ce atoms. From the analysis of the 3d XPS spectra we found that the occupation number of the 4f shell of Ce atoms is $n_f \approx 0.9$. The mixed valent character of Ce in CeRhGa was also confirmed by the magnetic data. Our band structure calculations gave a non-magnetic ground state of CeRhGa.

The low temperature specific heat data, $C(T)/T$, measured at different magnetic fields show a behaviour characteristic of a Fermi liquid state. At the external magnetic field $H = 0$ the Sommerfeld coefficient $C(T)/T = \gamma \sim 38$ mJ/mol K^2, that is typical for Ce-intermetallics with the 4f-shell instability. The Kondo temperature obtained from the $\gamma(T)$ at the zero external magnetic field is ~70 K, much smaller that the valence fluctuation temperature $T_{sf} \sim 500$ K.

The structure in which crystallizes CeRhGa is considerably simpler than the structure of similar CeRhAl compound [14]. It explains why complicated magnetic behaviour seen in CeRhAl [15] is not observed in CeRhGa, despite the fact that the shortest distances between Ce atoms are alike in both compounds (3.56 Å vs. 3.62 Å).

Acknowledgements

The authors thank the Polish Ministry of Science and Education for support from Project No. N N202 032137.

References

[1] A. Szytuła, J. Hrycyk, in: Crystal structures and magnetic properties of RTX rare earth intermetallics, Jagiellonian University Press, Kraków, 1998.
[2] F. Hulliger, J. Alloys Compd. 239 (1996) 131;
B. Chevalier, B. Heying, U.Ch. Rodewald, C. Peter Sebastian, E. Bauer, R. Pöttgen, Chem. Mater. 19 (2007) 3052.
[3] H. Wiesmann, M. Gurwitch, H. Lutz, A.K. Ghosh, B. Schwarz, M. Strongin, P.B. Allen, J.W. Halley, Phys. Rev. Lett. 38 (1977) 782.

[4] J. Rodriguez-Carvajal, Physica B. 192 (1993) 55.
[5] Elk FP-LAPW code, Kay Dewhurst, Sangeeta Sharma, Lars Nordström, Francesco Cricchio, Fredrik Bultmark, Hardy Gross, Claudia Ambrosch-Draxl, Clas Persson, Christian Brouder, Rickard Armiento, Andrew Chizmeshya, Per Anderson, Igor Nekrasov, Frank Wagner, Fateh Kalarasse, Jürgen Spitaler, Stefano Pittalis, Nektarios Lathiotakis, Tobias Burnus, Stephan Sagmeister, Christian Meisenbichler, Sébastien Lebégue, Yigang Zhang, Fritz Körmann, Alexey Baranov, Anton Kozhevnikov, Shigeru Suehara, Frank Essenberger, Antonio Sanna, Tyrel McQueen, Tim Baldsiefen, Marty Blaber, Anton Filanovich, Torbjörn Björkman http://elk.sourceforge.net/.
[6] J.P. Perdew, A. Ruzsinszky, G.I. Csonka, O.A. Vydrov, G.E. Scuseria, L.A. Constantin, X. Zhou, K. Burke, Phys. Rev. Lett. 100 (2008) 136406.
[7] J.J. Yeh, I. Lindau, Atom. Data Nucl. Data Tables 32 (1985) 1.
[8] B.C. Sales, D.K. Wohlleben, Phys. Rev. Lett. 35 (1975) 1240.
[9] J.M. Lawrence, P.S. Reiseborough, R.D. Parks, Rep. Prog. Phys. 44 (1981) 1.
[10] P.W. Anderson, Phys. Rev. B 124 (1961) 41.
[11] D.A. Shirley, Phys. Rev. 55 (1972) 4709.
[12] O. Gunnarsson, K. Schönhammer, Phys. Rev. B 28 (1983) 4315; J.C. Fuggle, F.U. Hillebrecht, Z. Zolnierek, R. Lässer, Ch. Freiburg, O. Gunnarsson, K. Schönhammer, Phys. Rev. B 27 (1983) 7330.
[13] N. Andrei, K. Furuya, J.H. Lowenstein, Rev. Mod. Phys. 55 (1983) 331.
[14] H. Schwer, F. Hulliger, J. Alloys Compd. 259 (1997) 249.
[15] A. Ślebarski, J. Goraus, A. Hackemer, M. Sołyga, Phys. Rev. B 70 (2004) 195123.